Int J Fract (2008) 154:61–72
DOI 10.1007/s10704-008-9270-y

ORIGINAL PAPER

Size effect on strength and fracture energy for numerical concrete with realistic aggregate shapes

Hau-Kit Man · Jan G. M. van Mier

Received: 30 May 2008 / Accepted: 8 October 2008

Abstract Fracture of concrete at the scale of the aggregate structure (or smaller) is a complicated process. Simple simulation models may be of help in understanding fracture in more detail, provided that the material structure is incorporated in as much detail as possible. A combined approach using computed tomography and image processing allows us to model concrete close to reality. The shape of the aggregates is included in a 3D beam lattice model for fracture. Fracture of concrete beams is simulated under 3-point bending with different sizes, aggregate densities and aggregates shapes, focusing on the size effect on structural strength and fracture energy.

Keywords Computed tomography · Aggregate structure · Oval-shaped aggregates · Crushed aggregates · Numerical concrete · 3D lattice model

1 Introduction

In this paper a size effect study is presented using numerical concrete. Lattice models are a suitable instrument for learning and understanding fracture mechanisms. The principle of the model is that the material is replaced by a network of one-dimensional, continuum line elements (springs, truss elements or beams).

Lattice type models were first studied by Hrennikoff (1941), who calculated linear elastic problems with truss elements in 2D, to some extent also in 3D (shells), long before computers were developed. Later statistical physics reintroduced the method for studying fracture (Herrmann et al. 1989) and was adopted and modified to study fracture in concrete (Schlangen and Van Mier 1992; Schlangen 1993). The lattice model was made suitable for concrete through various modifications including the use of triangular lattice geometries instead of using square lattices. This modification leads to an improved estimate of the Poisson's ratio. In addition an aggregate structure was implemented and different properties were assigned to elements falling in the respective material phases. In this model fracture is simulated by a removal of one beam element in each step.

On aggregate scale (millimeter scale) concrete has characteristically a high degree of heterogeneity. At this so-called meso-level concrete is usually characterized as a three-phase material, consisting of stiff aggregates, a weaker cement matrix and between them a weak interfacial transition zone. Variations may appear, for example low strength porous aggregates may be used in some cases, especially for reducing the density of the material. In that case concrete is still considered as a three-phase material, but the strength ratios are quite different compared to normal concrete.

H.-K. Man (✉) · J. G. M. van Mier
Department of Civil, Environmental and Geomatic Engineering (D-BAUG), Institute for Building Materials, ETH Zurich, 8093 Zurich, Switzerland
e-mail: hkman@ethz.ch

J. G. M. van Mier
e-mail: jvanmier@ethz.ch

In the lattice model, the heterogeneity can easily be included into the model by assigning different Young's modulus and tensile strengths, i.e. the material structure of concrete will be mapped into the mesh directly.

Lattice simulations were done initially in 2D with a relatively small number of around 3,000–30,000 lattice elements (see for example Schlangen and Van Mier 1992; Vervuurt 1997; Van Vliet 2000), which was limited primarily by the high demand on computational time.

Over the last years faster computing systems have developed rapidly. Moreover a parallel solver has been implemented in the lattice program, which allows to benefit from parallel computers (Lingen 2000). With this potential, high performance computers like the CRAY XT3 with over 1,656 computing processors can be used now for simulating fracture experiments. Thanks to this, analyses with a high number of lattice elements are possible. Fracture simulations can be carried out in full 3D (Lilliu and Van Mier 2003; Lilliu 2007; Man and Van Mier 2008; Van Mier and Man 2008), allowing building three-dimensional lattice networks with multi-million elements and a high degree of heterogeneity. At the same time the lattice element sizes are reduced, allowing including much more detail of the microstructure. For example the smallest element considered now was a lattice beam length of 0.1 mm. This was used to capture the structure of foamed cement in great detail, see Meyer et al. (2007).

The material structure of concrete can be generated with a computer program. In that case the aggregates are represented as circles in 2D or as spheres in 3D. In general a Fuller aggregate size distribution is used.

Recently, however, the material structure of concrete is modeled more realistically. The circular or spherical aggregates are still a simplification and one can argue that in reality the aggregates are generally non-spherical.

The geometries of aggregates vary and in practice aggregates with oval or crushed shapes are used (see Fig. 1a and b). For implementing those types of aggregates into the lattice model, a different kind of approach has to be developed. One possibility is to mathematically describe the shape of the aggregates, which was done for example by Wittmann et al. (1985) in 2D or by Garboczi (2002) in 3D. These descriptions are very complicated, but can be implemented into the already existing program. Nevertheless, this kind of approach lacks simplicity. Therefore instead of modifying and extending an existing computer program for generating the real grain structures, a different, but at the same time a very simple approach was designed.

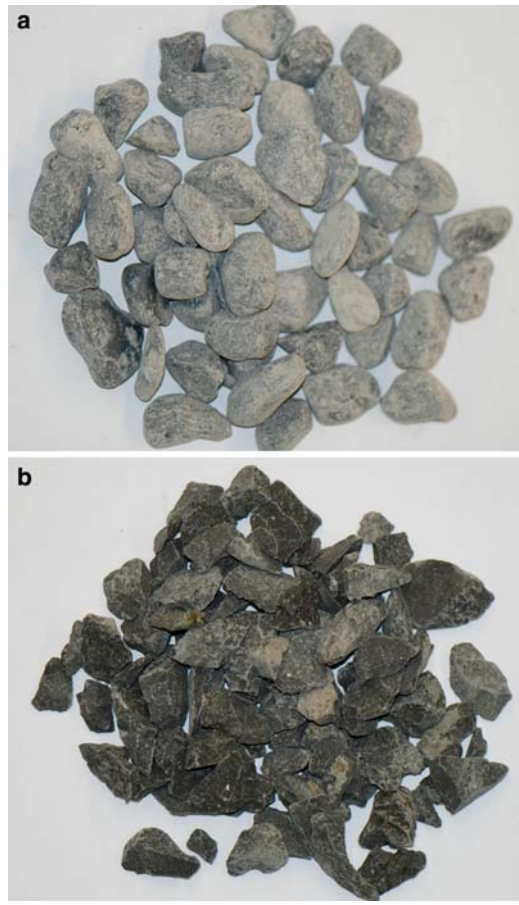

Fig. 1 Pictures of aggregates (basalt) used in the model concrete: (**a**) oval-shaped and (**b**) crushed aggregates

In this paper the new method will be introduced. CT-Scans of real concrete samples are modified to allow for direct mapping of the material structure onto a lattice. Examples of applications are shown. The focus is on the analysis is of the size effect on fracture strength and fracture energy (work of fracture).

2 Sample preparation and image processing

The basic concept of modeling real aggregate shapes is

- to extract the material structure directly from existing concrete samples and

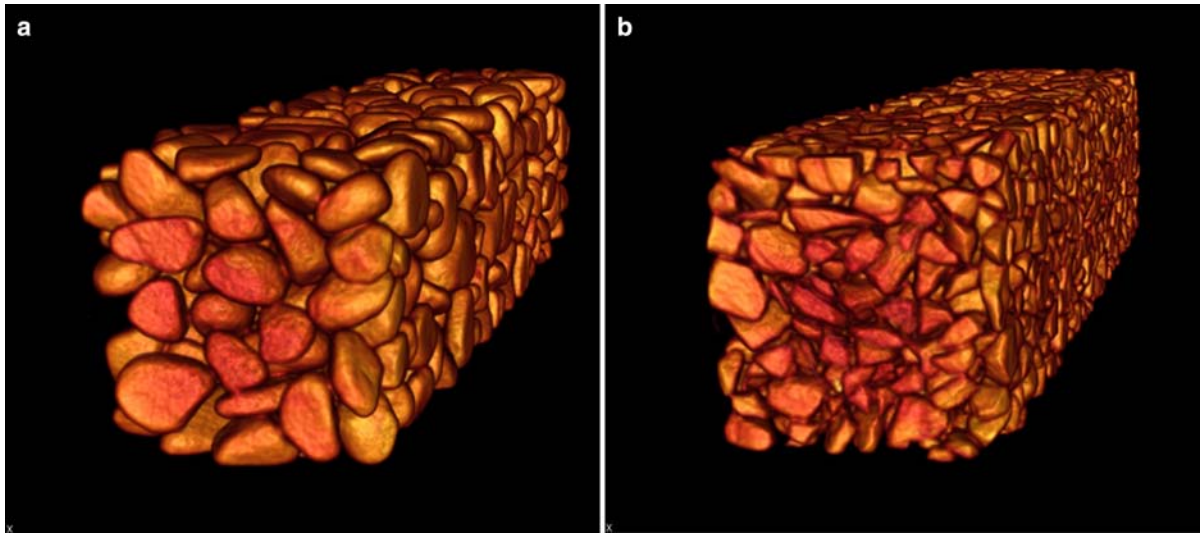

Fig. 2 Microstructure of a scanned concrete prism after CT scan (volume rendering): (**a**) oval-shaped and (**b**) crushed aggregates

- to transfer this structural information directly into the lattice model.

To detect the aggregates structure of real concrete structures, prisms are scanned through computed tomography (CT-scan). The resulting images serve as basis for implementing the aggregate structure into the numerical model. This approach has the obvious advantage of using real instead of computer-generated spherical aggregates.

Concrete specimens are prepared with cement CEM I 42.5 with a low water-cement ratio (w/c = 0.3 by weight) and with aggregates, which have either oval or crushed shapes. Different kinds of aggregates were selected and scanned: basalt and marble. These two materials have a much higher density in comparison to the cement matrix, and are thus suitable for experiments in the CT scanner. Cement matrix with a w/c ratio of 0.3 has a density of around 2,100–2,200 kg/m^3, while basalt has a density of around 3,000 kg/m^3 and marble of around 2,700 kg/m^3. The used aggregates are shown in Fig. 1.

All the concrete prisms were scanned with a medical dual source CT scanner Siemens SOMATOM Definition. The result of the scanning process is a series of 2D images, which can be reconstructed in various ways. A volume of a concrete specimen can be built simply by 'stacking' the individual slices one on top on one another. This is a technique called "volume rendering" (see Fig. 2a and b). A similar technique will be applied to map the material structure into the lattice model.

To transfer/map this information of the microstructure directly into the lattice model, the slices of the images will be overlaid directly on the respective nodes. Usually low-density materials are in dark tones (cement matrix) and material with a high density like the aggregates are represented in lighter tones (see Fig. 3). By stacking the individual slices into the third dimension (analog to volume rendering) a 3D microstructure is generated. In addition to build a 3D lattice model the nodes must be connected into a lattice network.

To determine the material property of a lattice element, a simple procedure checks whether both nodes fall within an aggregate particle: the element will be assigned aggregate properties. If both nodes are within the cement matrix, the element will be assigned cement matrix properties, whereas when the element has one aggregate and one matrix node it will be assigned ITZ (interfacial transition zone) properties.

Figure 3 shows a comparison of one slice of the scanned image and the resulting lattice model. The lattice shows the three phases: cement matrix (blue), aggregates (red) and ITZ (green). The figure illustrates clearly that the shapes of the aggregates from the real samples can be captured in the lattice structure quite well and non-spherical aggregate shapes can be modeled by means of this simple approach.

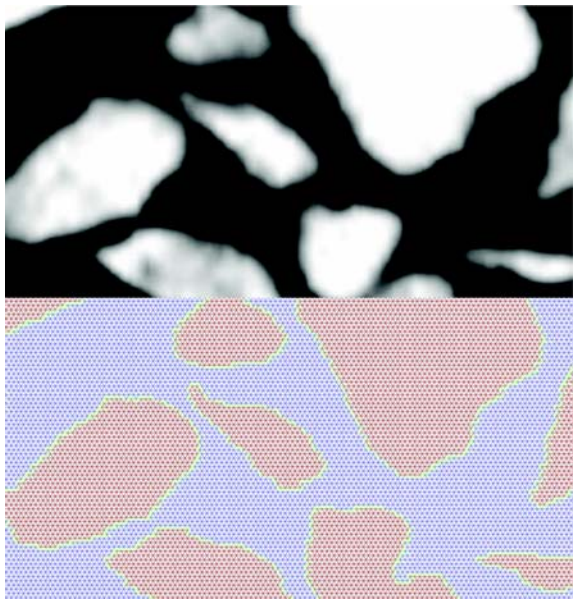

Fig. 3 Comparison of the microstructure from a X-ray tomography slice with a slice of a 3D lattice

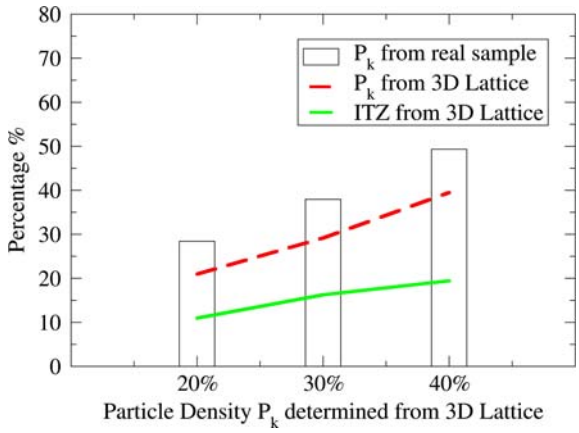

Fig. 4 Comparison between the P_k of a real concrete sample with the lattice structures for $P_k = 20\%$, 30 and 40% (with the element size C "large" with 1,155,549 lattice elements)

It seems that this method is applicable for modeling real concrete structures including as much detail as required. Figure 4 makes a quantitative comparison between the scanned concrete samples and the resultant lattice structure. The comparison was done on three samples with crushed shaped aggregates. The comparison in Fig. 4 shows that the lattice structure has a lower aggregate volume P_k. In all models the P_k-ratio of the (numerical) concrete is underestimated:

$$P_k(\text{real concrete sample}) > P_k(\text{3D lattice}). \quad (1)$$

The aggregate volume of the scanned specimen is 5–8% higher than its numerical counterpart. The difference is explained from the integration of the ITZ, which has a thickness of exactly one-lattice element length. This is dearly an overestimation, since in reality the ITZ thickness should be in the order of 20–40 μm (Scrivener 1989). To solve this problem there are several possibilities: either reducing the length of ITZ beams or reducing the length of all lattice beams in general; in both cases this would raise the element numbers and consequently increase the computational time. In the end a reasonable balance must be derived between spatial resolutions and computational effort needed.

In the analysis presented in this paper we have kept the same beam length for the entire lattice.

3 Simple lattice model

The lattice model, which is used here, is based on a sequential removal of one Bernoulli beam in each step: simulating the fracture process of concrete with this model is (still) very time-consuming and the need of computational resources is huge. Nevertheless for understanding the fracture process of quasi-brittle materials such as concrete it appears to be a simple and useful method. The fracture law has the following form:

$$\frac{\sigma}{f_t} = \frac{1}{f_t}\left(\frac{N}{A} + \alpha\frac{\max(M_i, M_j)}{W}\right) \quad (2)$$

with N the normal force, A the cross-section area, M_i the bending moment of the node i and W the sectional modulus. f_t is the tensile strength of the considered lattice element. The parameter α determines the role of bending in the fracture law.

In our case we choose $\alpha = 0$, thus reducing the fracture criterion into a simple maximum tensile stress criterion which resembles the Rankine criterion. This same assumption was made in earlier 3D lattice analysis (Lilliu and Van Mier 2003; Lilliu 2007). Thus, Eq. 2 reduces into the much simpler expression:

$$\frac{\sigma}{f_t} = \frac{1}{f_t}\frac{N}{A} \quad (3)$$

In each sequential step the element with the highest $\frac{\sigma}{f_t}$ value will be removed from the lattice mesh.

4 Overview of the analysis

In this paper, fracture simulations are presented on concrete prisms subjected to 3 point bending. The prisms have varying particle densities, different aggregate shapes and different sizes. In the present size effect study the specimen sizes will be scaled in all three directions. The size ratio from the smallest to the largest specimen is 1:8 (see Table 1).

In the past size effect studies scaling the specimen size was commonly done in two dimensions only (scaling in length and height). One size parameter is held constant which is usually the thickness. This approach (referred to 2D scaling) is, in contrast to 3D (or full) scaling, a much simpler and less demanding approach, both, in experiments and numerical simulations. The specimen volume increases by a factor 2^n, assuming a doubling with $n = 2$ in 2D and $n = 3$ in 3D. It is obvious that the volume (and thus at the same time the number of elements required) in 3D scaling increases significantly compared to 2D scaling.

There are some advantages of using 3D scaling over 2D scaling. In 3D scaling usually a three-dimensional material structure is used, for example the aggregates are modeled fully in 3D, while in two-dimensional scaling the material structure is also represented in 2D, which means that the aggregates are modeled either as circles (plane stress) or as cylinders (plane strain).

As mentioned above in 2D scaling the specimen thickness is held constant for all specimen sizes. If the thickness is significantly smaller than the two other specimen dimensions, a plane-stress analysis will suffice. The situation changes when the thickness is of the same order as the other specimen dimensions and a plane-strain analysis is required. This is not entirely clear where the transition lies.

Another aspect is that wall effects can be included in a 3D analysis. Depending on whether a concrete specimen is cast or sawn from a larger block, different wall effects exist. Walls are in a 3D case two-dimensional planes, whereas in the 2D case walls are represented by one-dimensional lines only.

The lattice element numbers ranges from 21,107 to 9,269,081 elements, from the smallest specimen size ($6.25 \times 2.38 \times 2.6$ mm) to the largest ($50 \times 18.84 \times 19.04$ mm, see Table 1). A regular triangular lattice configuration was used with a beam length of 0.25 mm, which is used for all prism sizes. The ratio of the Young's modulus of the aggregate, cement matrix and the ITZ phases is: 70/25/25; the ratio of the tensile strengths is 10/5/1.25.

Due to the improvements of modeling the microstructure mentioned earlier, the shapes of the aggregates can be either oval or crushed. For the rough particles three different particle densities were investigated: $P_k = 20$, 30 and 40% (see Fig. 5a–c).

To compare between rough and oval shaped aggregates directly and to find out structural and mechanical differences, also a concrete specimen with oval shaped aggregates and $P_k = 40\%$ was selected and analyzed (Fig. 5d). The aggregate size ranges between 1.5 and 3 mm. To obtain a similar microstructure, it is convenient to use one large scanned concrete prism and to cut all specimens from this large microstructure.

Figure 6 shows four lattices of different sizes containing crushed aggregates ($P_k = 20\%$). The material structure are kept the same, see the circled area on the figures. In the center of one edge the material structure is identical for all sizes. For the remainder of the specimen there is un-avoidable variation.

The largest specimen size was simulated only once, the second largest size was repeated 5–6 times, the medium size 8–10 and for the smallest one 10–12 simulations were performed (see Table 2).

These fracture simulations are performed on different computers: either on small unix/linux workstations with up to four processors, mid-size computing servers (SGI Altix 350 with 16 Intel Itanium 2 processors and 32 GB of shared memory) to larger servers (HP Superdome with 96 Intel Itanium 2 dual-core

Table 1 Specimen size and number of lattice elements

	A	B	C	D
# Lattice elements	21,107	143,627	1,155,549	9,269,081
Specimen size (mm)	$6.25 \times 2.38 \times 2.6$	$12.5 \times 4.6 \times 4.8$	$25 \times 9.31 \times 9.53$	$50 \times 18.84 \times 19.04$

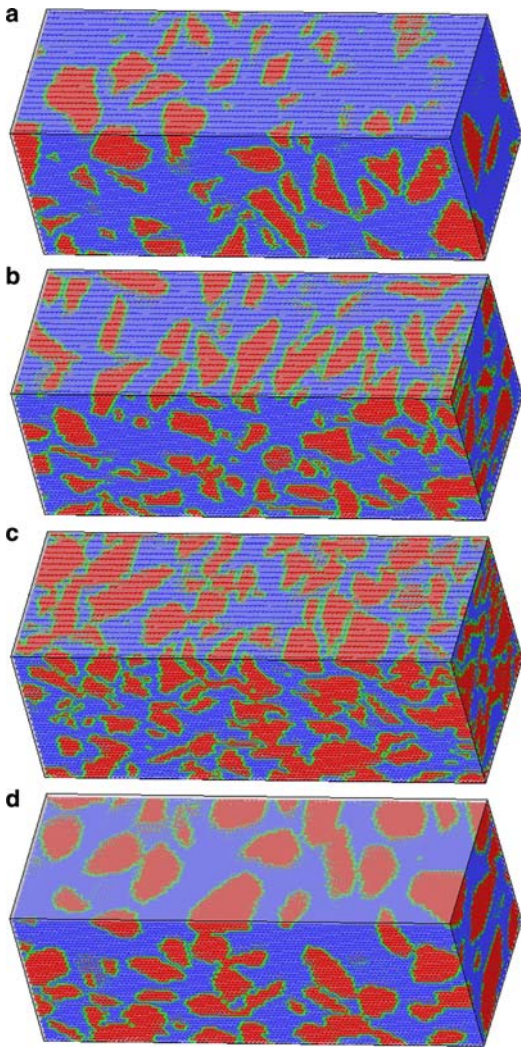

Fig. 5 Microstructure of the four concrete prisms with P_k = 20% (**a**), 30% (**b**), and 40% (**c**), with crushed aggregates, P_k = 40% with oval-shaped aggregates (**d**). The specimen size is C ("Large")

processors and 384 GB of shared memory) and massive parallel computing facilities like the CRAY XT3 from the Swiss National Supercomputing Center, which has a total of 1,656 AMD Opteron dual-core processors with 2GB RAM per processor (total of 3,312 processing cores). It proved to be optimal to use 64–256 processors in the CRAY XT3. This facility was used to analyse the two largest specimen sizes (specimen size C with 1,155,549 and size D with 9,269,081 elements).

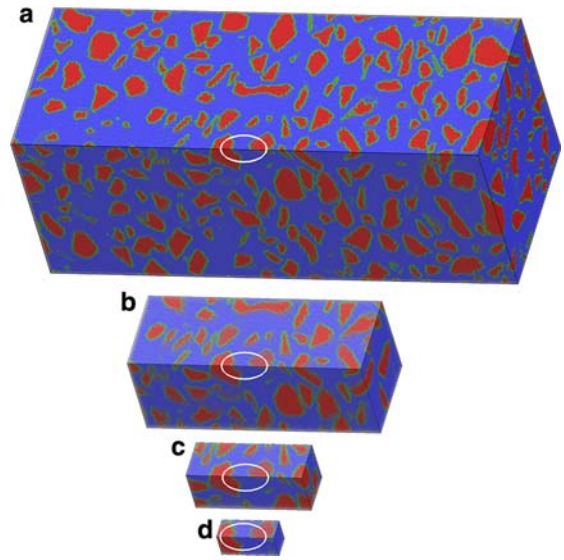

Fig. 6 Microstructure of 3D lattices with P_k = 20%, from the largest (**a**) to the smallest specimen (**d**). The circled area indicates where the microstructure matches

5 Structural study

Figure 7 compares the distribution of the material phases between oval and crushed aggregates with $P_k = 40\%$. The smallest specimen with $P_k = 40\%$ (in both cases) is not exactly matched (an average of $P_k = 34\%$ for concrete with oval aggregates and $P_k = 44\%$ for crushed aggregates with a large errorbar), which is in contrast to the larger sizes, that converge to the original P_k of 40% and also the errorbars are much smaller. As mentioned, the smallest specimen size is $6.25 \times 2.38 \times 2.6$ mm and the grain size ranges between 1.5 and 3 mm. One can argue that this is probably the main problem here; the biggest aggregate is not significantly smaller than the prism size. In our case it is not unusual to have only 2–3 aggregates in such a small specimen (see for example Fig. 6d), therefore

Table 2 Number of simulations done for each case

	A (small)	B (medium)	C (large)	D (xlarge)
20% (crushed aggregates)	10	10	6	1
30% (crushed aggregates)	12	8	5	1
40% (crushed aggregates)	12	8	6	1
40% (oval-shaped aggregates)	12	8	5	1

it is very difficult to match the same P_k in comparison to the larger sizes. One can certainly discuss if the smallest specimen size should be included in the analysis at all, but by doing so one has also to consider that the size ratio from the smallest to the largest prism size would be only 1:4 instead of 1:8. It was decided to keep the smallest size in our analysis, but running more simulations for the smallest sizes compared to the larger ones.

This discrepancy of the P_k of the smallest compared to the larger sizes and the large scatter of aggregate density for the smallest size can also be observed for the other cases as well (see Table 3).

Although Fig. 7 shows that both aggregate types have a comparable P_k of around 40%, the number of ITZ elements differs significantly. With identical P_k, the crushed aggregates have a higher number of ITZ elements in comparison to the oval shaped aggregates, at the same time a lower share of cement matrix elements.

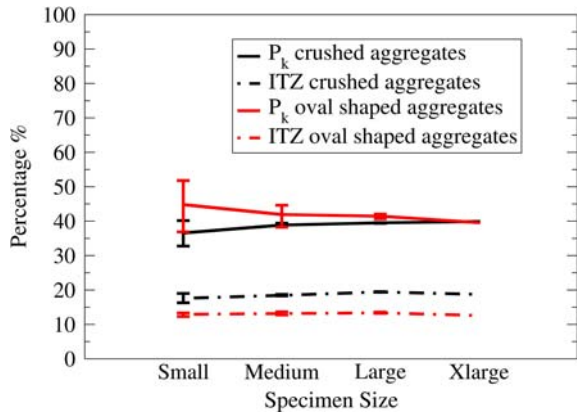

Fig. 7 Comparison of oval and crushed aggregates at $P_k = 40\%$

Table 4 indicates that the difference on ITZ elements are up to 46% for the second largest specimen size, concluding that crushed aggregates have a higher specific surface, as was expected.

Table 3 Numbers of elements used in the various computations with the distribution of the three material parameters. Standard-deviation in brackets

	Average # Agg.	# ITZ	# Matrix	% Agg.	% ITZ	% Mat.
$P_k = 40\%$ *(oval-shaped aggregates)*						
A	9,457 (1,062)	2,731 (71)	8,919 (1,011)	44.81	12.94	42.26
B	60,224 (3,676)	18,893 (604)	64,509 (4,132)	41.93	13.15	44.91
C	479,039 (6,244)	154,455 (1,825)	522,055 (7,876)	41.46	13.37	45.18
D	3,669,629 (–)	1,167,904 (–)	4,431,548 (–)	39.59	12.6	47.81
$P_k = 40\%$ *(crushed aggregates)*						
A	7,221 (530)	3,713 (186)	9,674 (495)	36.58	17.59	45.83
B	55,840 (476)	26,516 (283)	61,271 (610)	38.88	18.46	42.66
C	456,612 (976)	224,790 (914)	473,096 (1,317)	39.51	19.45	41.03
D	3,891,140 (–)	1,519,241 (–)	3,858,700 (–)	41.97	16.39	41.63
$P_k = 30\%$ *(crushed aggregates)*						
A	7,216 (1,018)	3,632 (215)	10,259 (1,022)	34.19	17.21	48.60
B	43,475 (3,093)	23,956 (1,114)	76,195 (4,036)	30.27	16.68	53.05
C	337,039 (2,904)	187,919 (435)	630,591 (3,206)	29.17	16.26	54.57
D	2,833,558 (–)	1,475,637 (–)	4,959,886 (–)	30.57	15.92	53.51
$P_k = 20\%$ *(crushed aggregates)*						
A	4,824 (1,313)	2,239 (297)	14,046 (1,366)	22.85	10.61	66.54
B	35,110 (1,350)	16,397 (1,320)	92,150 (2,067)	24.69	11.65	63.66
C	242,385 (13,548)	127,040 (3,369)	786,124 (16,910)	20.98	11.99	68.03
D	2,037,206 (–)	1,045,543 (–)	6,186,332 (–)	21.98	11.28	66.74

Table 4 Comparison of the numbers of ITZ elements between concrete containing crushed aggregates or oval-shaped aggregates at $P_k = 40\%$

	Average # of ITZ elements crushed aggregates	Average # of ITZ elements oval-shaped aggregates	Ratio
A	3,713	2,731	1.35
B	26,516	18,893	1.40
C	224,790	154,455	1.46
D	1,519,241	1,167,904	1.3

6 Fracture behavior

Figures 8 and 9 illustrate the fracture behavior for both crushed and oval-shaped aggregates (with $P_k = 40\%$) at 3 different stages (marked in the respective load displacement diagram) for specimens of size C ("Large"). Figures 8a and 9a illustrate the fracture pattern at maximum load, Figs. 8b and 9b during softening and Figs. 8c and 9c at the end of the softening stage. Figures 8d and 9d are the load-displacement diagrams for each case. The load displacement diagram shows the zig-zag curves, which is characteristic for lattice type simula-

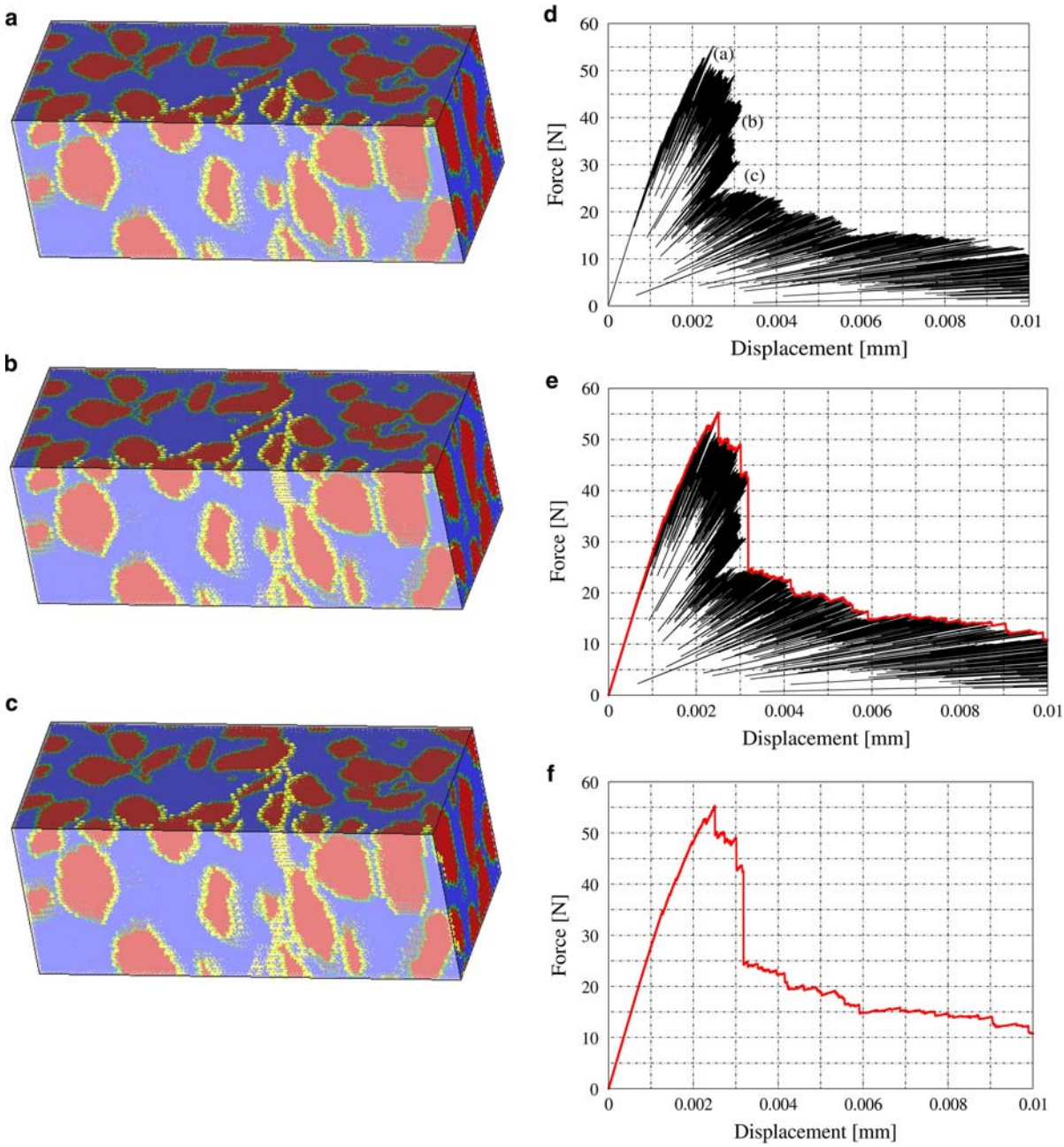

Fig. 8 Fracture process of a 3D lattice with oval-shaped aggregates at different stages

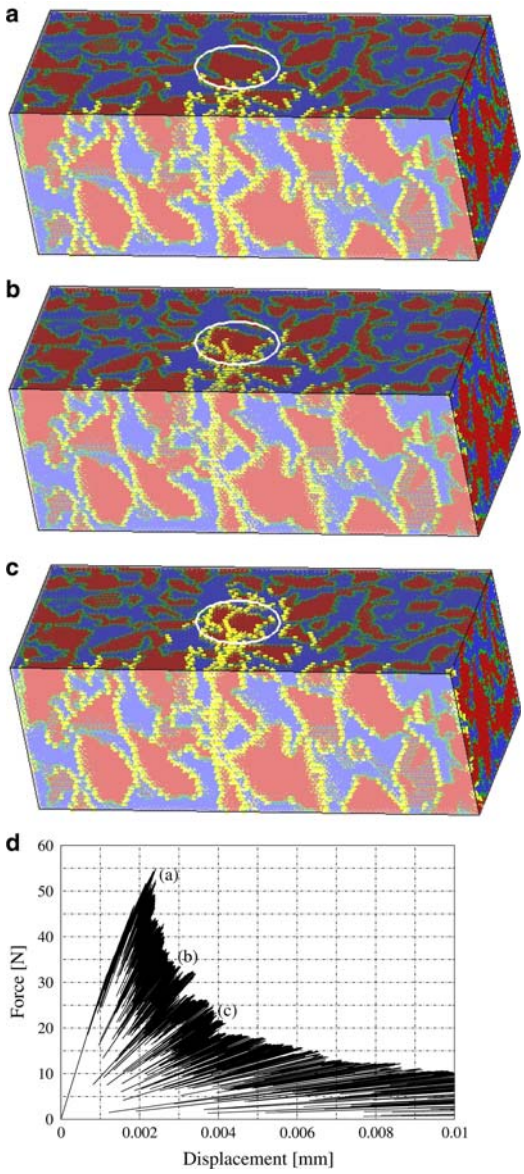

Fig. 9 Fracture process of a 3D lattice with crushed aggregates at different stages. The circled area shows an example of an aggregate crack

tions, reflecting the subsequent loading-unloading curves upon lattice element removal. Nevertheless the envelope curve (Fig. 8f) of the fracture simulation is similar to the typical fracture behaviour of concrete observed in experiments.

One fracture simulation on concrete with oval aggregates is illustrated in Fig. 8. In the beginning microcracks develop along the interface zone. Until peak load interface cracks appear predominantly. After reaching maximum load macrocracks grow through the cement matrix and finally deformations localize in one large single crack (Fig. 8c). Fracture occurs usually only in the bond zone and in the cement matrix.

The analysis of the fracture process of concrete with crushed aggregates (Fig. 9) shows that until peak-load the microcracks develop in the same way as in the example of Fig. 8 with oval-shaped aggregates. However after maximum load, different fracture behaviour is visible. Figure 9b and c show that fracture can also occur through the aggregate. The circled area of Fig. 9a–c points that out. This is unusual because aggregates have a two times higher tensile strength in comparison to the cement matrix and an eight times higher strength than ITZ. The present analyses show that aggregate fracture is possible for extreme aggregate shapes. In contrast fracture simulations with spherical aggregates and also with oval shaped aggregates usually do not show any aggregate fracture.

7 Size effect on structural strength

Size effect on structural strength is typically shown by calculating the nominal bending (or tensile) stress and illustrating that in a bi-logarithmic diagram containing the stress on one axis and the characteristic specimen size along the other. Alternatively a different formulation is postulated in Man and Van Mier (2007), who proposed using a double-logarithmic nominal strength vs. specimen volume relationship instead.

Figure 10a and b show that the bending strength decreases with increasing specimen size, which is in agreement with many other the studies. Through linear regression, which has the following form:

$$\ln \sigma = \mathrm{a} + \mathrm{b} \ln \mathrm{H}, \tag{4}$$

where σ is the nominal bending strength and H is the characteristic specimen size (in this case the specimen height), the four curves can be presented in a simple manner. The calculated values for a, b (b indicates the slope of the regression curve) are in Table 5a and b. In Table 5a, the slopes are calculated for the smallest to the largest specimen (A–D), in Table 5b for size B–D.

For the crushed shaped aggregates the slopes varies are between −0.5 and −0.58, depending on P_k. In the case with oval-shaped aggregates the slope is −0.58, which is close to the linear elastic fracture mechanics solution of −0.5. The diagram on Fig. 10b shows

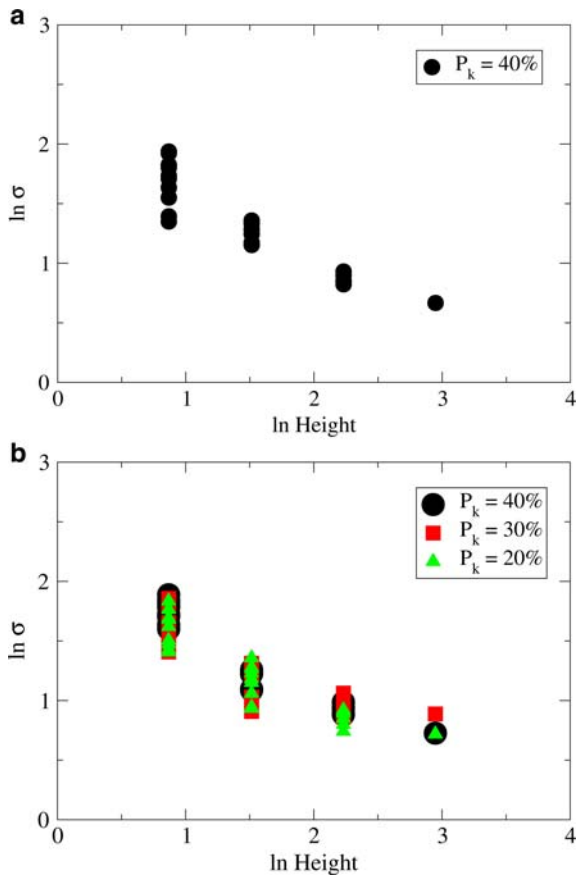

Fig. 10 Bi-logarithmic nominal strength vs. specimen height relationship of concrete: (**a**) $P_k = 40\%$ with oval-shaped aggregates, (**b**) $P_k = 20\%$, 30 and 40% with crushed aggregates

non-linear behavior on the bi-logarithmic diagram, showing the slopes are not constant and become flatter with increasing size.

So if one takes a closer look into the three largest sizes only, as indicated in the past (because the P_k of the smallest specimen does not match the P_k of the other sizes), the slopes change. For the crushed aggregates it decreases from $b = -0.22$ to $b = -0.37$, whereas for the oval-shaped aggregates $b = -0.48$. In all cases the slopes are flatter. In the case of concrete structures with oval-shaped aggregates the LEFM assumption may be correct; in the case of the crushed aggregates, the slopes are close to the Weibull theory assuming that the Weibull modulus is $m = 12$ for concrete, suggested by Zech and Wittmann (1978). One explanation of the change of slope is the large scatter of the bending strength for the smallest specimen size. The largest grain size is 3 mm and the specimen height is 2.6 mm only, resulting in a height over grain size ratio below 1. The specimen size A is clearly too small to be representative for the material.

8 Work of fracture (fracture energy)

The fracture energy is considered as a material parameter by some researchers (Duan et al. 2007). From that standpoint it should be a size-independent constant.

For the present simulations the work of fracture can be obtained from the following equation:

$$W = \frac{1}{bh} \int P d\delta. \tag{5}$$

P is the measured force and δ the displacement. The integral can be evaluated from the area under the load-displacement (P-δ) curve. It has to be noted that the envelope curve was taken to calculate the fracture energy, thus neglecting the zigzags (Fig. 8f). The integral is then averaged over the area of the specimen height h and thickness b.

Figure 11 illustrates the calculated work of fracture for the four cases. On average the fracture energy on

Table 5 Coefficients of the regression analysis from Eq. 4. (a) Regression analysis from size A to D. (**b**) Regression analysis from size B to D

	a	b	R^2
a			
20% (crushed aggregates)	1.98	−0.5	0.82
30% (crushed aggregates)	1.93	−0.45	0.79
40% (crushed aggregates)	2.18	−0.57	0.86
40% (oval-shaped aggregates)	2.18	−0.58	0.85
b			
20% (crushed aggregates)	1.7	−0.37	0.73
30% (crushed aggregates)	1.47	−0.22	0.72
40% (crushed aggregates)	1.54	−0.26	0.79
40% (oval-shaped aggregates)	1.99	−0.48	0.88

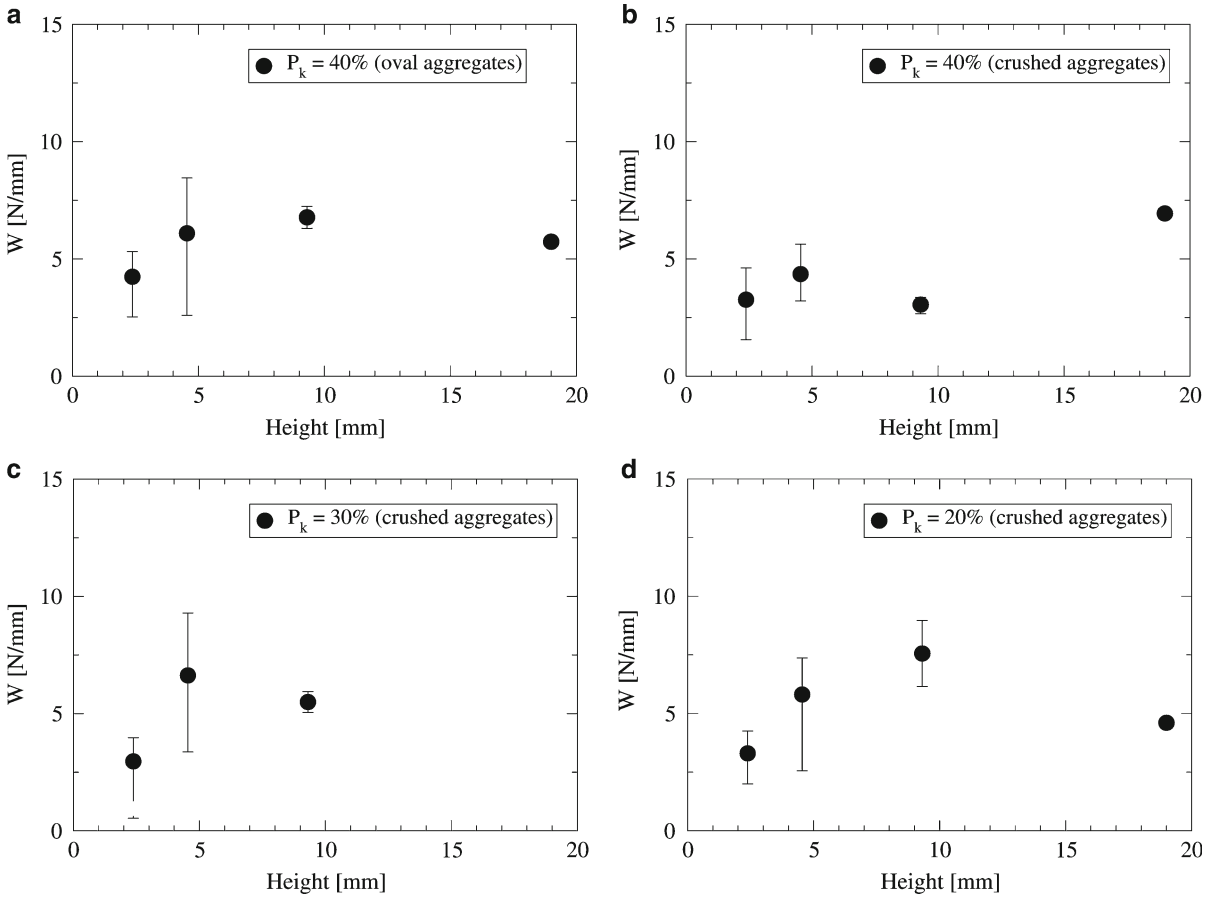

Fig. 11 Calculation of the total work of fracture for different sizes and different P_k: (**a**) $P_k = 40\%$ with oval-shaped aggregates, (**b**) $P_k = 40\%$, (**c**) $P_k = 30\%$ and (**d**) $P_k = 40\%$ with crushed aggregates

concrete with oval-shaped aggregates is higher in comparison to those with crushed aggregates. The fracture energy varies with size, the minimum specific fracture energy usually at the smallest size, which is observed also for the case of $P_k = 20\%$ and 30% (Fig. 11c and d). More computations are needed for the two larger sizes to find out if the curves are approaching a certain asymptotic value, as was observed in experiments (Van Vliet and Van Mier 2000).

9 Summary and conclusions

In this paper results are presented from a study on the size effect on fracture of (numerical) concrete subjected to 3 point bending. Scaling was done in all three directions for prisms of four different sizes; the ratio from the largest to the smallest specimen size is 8.

Fracture simulations were performed with a three-dimensional lattice model, with multi-million lattice beam elements.

One of the improvements made is that the concrete microstructure can now be modeled more accurately than in the past. At the aggregate level concrete generally has random geometries (shapes). Instead of using ideal spherical aggregates like in the past, a procedure was developed to transfer the results from X-ray scans of concrete directly into the 3D lattice. As a result concrete is modeled more realistically at the aggregate level; real shapes of aggregate particles are included into the lattice model, like, for example, oval-shaped or crushed (broken) aggregates.

The comparison of the fracture behavior of concrete with oval-shaped and crushed aggregates shows significant differences. Fracture of concrete with oval-shaped (also with ideal spherical) aggregates occurs along the bond zones and in the cement matrix (fracture in two

phases), whereas in concrete structures with crushed aggregates cracks also appear through the aggregates (fracture in all three phases).

The study showed that the bending strength varies with size. The slope of the regression curves in a bi-logarithmic nominal stress—size diagram appear to change with size and is not a constant. Concrete with crushed aggregates has a slope close to the LEFM limit of -0.5, if considering all sizes. When only the three largest specimen sizes are considered the slope becomes flatter.

The results obtained indicate that it seems to be useful to study at least one additional size; i.e. the next larger one. The next larger prism has the length of $100 \times 39 \times 38$ mm with a total of 74,248,497 lattice elements, thus a considerable numerical effort is needed.

Acknowledgements The authors would like to thank Tino Tschenett and Stephan Simioni who took part of the size effect study during their BSc thesis (Simioni and Tschenett 2007), supervised by the authors. The CT scans of the concrete samples were performed at the University Hospital in Zurich. Most of the simulations, especially the fracture experiments of the two largest specimen sizes, were carried out on the CRAY XT3 at the Swiss National Supercomputing Center (CSCS) in Manno (TI), Switzerland. The support of the University Hospital and CSCS is gratefully acknowledged.

References

Duan K, Hu X, Wittmann FH (2007) Size effect on specific fracture energy of concrete. Eng Fract Mech 74:87–96

Garboczi EJ (2002) Three-dimensional mathematical analysis of particle shape using X-ray tomography and spherical harmonics: application to aggregates used in concrete. Cem Concr Res 32:1621–1638

Herrmann HJ, Hansen A, Roux S (1989) Fracture of disordered elastic lattices in two dimensions. Phys Rev B 39(1): 637–648. doi:10.1103/PhysRevB.39.637

Lilliu G (2007) Analysis of 3D fracture processes in concrete. PhD thesis, TU Delft

Lilliu G, van Mier JGM (2003) 3D lattice type fracture model for concrete. Eng Fract Mech 70:927–941. doi:10.1016/S0013-7944(02)00158-3

Lingen FJ (2000) Design of an object-oriented finite element package for parallel computers. PhD thesis, TU Delft

Man H-K, Van Mier JGM (2007) Size and shape effects of fracture strength of concrete. In: Carpinteri A, Gambarova P, Ferro G, Plizarri G (eds) Fracture mechanics of concrete and concrete structures (FraMCoS-6). Taylor & Francis Group, London, pp 39–44

Man H-K, Van Mier JGM (2008) Influence of particle density on 3D size effects in the fracture of (Numerical) concrete. Mech Mater 40:470–486

Meyer D, Man H-K, Van Mier JGM (2007) Fracture of foamed cementitious materials: a combined experimental and numerical study. In: Zhao H, Fleck NA (eds) Proceedings IUTAM symposium on 'mechanical properties of cellular materials', LMT-Cachan, Paris, France, September 17–21, 2007. Kluwer Academic Publishers, Dordrecht (in press)

Schlangen E (1993) Experimental and numerical analysis of fracture processes in concrete. PhD thesis, TU Delft

Schlangen E, van Mier JGM (1992) Experimental and numerical analysis of micromechanism of fracture of cement based composites. Cem Concr Compos 14:105–118. doi:10.1016/0958-9465(92)90004-F

Scrivener K (1989) The microstructure of concrete. In: Skalny IJ (ed) Materials science of concrete. The American Ceramic Society Westerville, OH, p 127

Simioni S, Tschenett T (2007) Analysis of size-effects on fracture strength for concretes containing realistic aggregate particles. BSc thesis, Department of Civil, Environmental and Geomatic Engineering, ETH Zurich

Van Mier JGM, Man H-K (2008) Some notes on microcracking, softening, localization and size effects. Int J Damage Mech. Special Issue in memoriam of D. Krajcinovic (in press)

Van Mier JGM, van Vliet MRA, Wang TK (2002) Fracture mechanisms in particle composites: statistical aspects in lattice type analysis. Mech Mater 34(11):705–724. doi:10.1016/S0167-6636(02)00170-9

Van Vliet MRA (2000) Size effect in tensile fracture of concrete and rock. PhD thesis, TU Delft

Van Vliet MRA, Van Mier JGM (2000) Experimental investigation of size effect in concrete and sandstone under uniaxial tension. Eng Fract Mech 65(2–3):165–188

Vervuurt A (1997) Interface fracture in concrete. PhD thesis, TU Delft

Weibull W (1939) A statistical theory of the strength of materials. Roy Sweden Acad Eng Sci Proc 151:1–45

Wittmann FH, Roefstra PE, Sadouki H (1985) Simulation and analysis of composite structures. Mater Sci Eng 68: 239–248

Zech B, Wittmann FH (1978) A complex study on the reliability assessment of the containment of a PWR. Part II, Probalistic approach to describe the behaviour of materials. Nucl Eng Des 48:563–593. doi:10.1016/0029-5493(78)90099-7